and/or that these amide protons are in a hydrophobic environment excluded from solvent molecules. Verification that the chemical shift (7.98 ppm) remaining after 12 h of hydrogen-deuterium exchange (Figure 9D) belongs to the Leu-12 amide rather than the Glu-15 amide was obtained by a HOHAHA 2D-NMR spectrum recorded between 7 and 12 h after the peptide was dissolved in D_2O/TFE-d_3. Recently, Ciesla et al.[50] observed a similar amide-exchange effect on a peptide which formed a four-helix bundle. They found that the hydrogen-deuterium exchange rate of the amide proton was decreased as the amide position was changed from end to central positions of the peptide, and these results can be explained if intermolecular association protects the amide protons from deuterium in the solvent.[48] However, the difference in exchange rates of different amides from this study cannot be explained by secondary structural differences or by intermolecular association, because it has been clearly demonstrated that the peptide LL9 is highly α-helical (CD and NMR studies) and is monomeric in 50% TFE (size-exclusion chromatography) and that the ellipticities at 220 nm are independent of peptide concentration (0.038-4.9 mM), suggesting no intermolecular association in 50% TFE.[29,35,51] The most plausible explanation is that this helical peptide has a time-averaged curvature with the hydrophobic face being concave, which results in the hydrophobic side chains in the center of hydrophobic face forming a hydrophobic microenvironment which protects the amide in this region from deuterium exchange with solvent molecules. The slow-exchange amides (Leu-13, Leu-9, Leu-6, Leu-12, and Glu-10) are all located in the center of hydrophobic face (Figure 6).

(50) Ciesla, D. J.; Gilbert, D. E.; Feigan, J. *J. Am. Chem. Soc.* **1991**, *113*, 3957-3961.
(51) Lyu, P. C.; Liff, M. I.; Marky, L. A.; Kallenbach, N. R. *Science* **1990**, *250*, 669-673.

Conclusions

This study has provided new insights into the relationship between amide chemical shifts and α-helical structure and demonstrated that the change in the amide chemical shift in an α-helix is not caused by the α-helical structure itself but is due to the amphipathic nature of the α-helix. These results suggest that the amide proton chemical shift is related to hydrogen-bond length and that a single-stranded amphipathic α-helix in solution is curved and this curved structure causes the upfield shifts of the amide protons in the convex side and the downfield shifts of the amide protons in the concave side. Understanding the relationship between the amide chemical shift and hydrogen-bond distance in an α-helical structure will have major implications in the studies of protein folding, protein-ligand binding, and protein-protein interactions, if these processes involve hydrogen bonds.

Acknowledgment. This project is an integral part of the Protein Engineering Network of Centres of Excellence Program supported by the Government of Canada. A postdoctoral fellowship stipend (N.E.Z.) and research allowance were provided by the Alberta Heritage Foundation for Medical Research. We thank Paul D. Semchuk and David Clarke for their assistance in peptide synthesis and purification and Bob Luty and Linda Golden for their skilled technical assistance in performing circular dichroism and NMR measurements.

^{13}C-$\{^1H\}$ NMR/NOE and Multiplet Relaxation Data in Modeling Protein Dynamics of a Collagen ^{13}C-Enriched Glycine GXX Repeat Motif Hexadecapeptide[‡,†]

Vladimir A. Daragan[§] and Kevin H. Mayo*

Contribution from the Structural Biology Group, Department of Pharmacology, The Jefferson Cancer Institute, Thomas Jefferson University, Philadelphia, Pennsylvania 19107.
Received August 15, 1991

Abstract: ^{13}C-NMR (75 MHz) multiplet spin-lattice (T_1) relaxation and ^{13}C-$\{^1H\}$ nuclear Overhauser measurements have been performed on a ^{13}C-glycine-XX repeating hexadecapeptide, i.e., GVKGDKGNPGWPGAPY, from the triple helix domain of collagen type IV. The data have been analyzed using a formalism that considers both autocorrelation and cross-correlation dipolar spectral densities. Several motional models were tested for consistency with the data. The terminal glycine, G1, and nonterminal glycines, G4, G7, G10, and G13, were found to have distinctly different motional properties that could not be explained simultaneously by any one model. Results indicate that most glycines rotate more isotropically than the N-terminal glycine. Analysis of the experimental data using several rotational models indicates that internal motions in the peptide are important to terminal, as well as nonterminal, ^{13}C-glycine relaxation. The character of the rotational motion of nonterminal glycines varies considerably with temperature. Although simple rotational diffusion models can describe terminal glycine motion, consideration of multiple internal rotations are necessary to fully describe nonterminal glycine rotations.

Introduction

Over the last 10 or so years, the functional significance of protein structural dynamics/internal motions in biological activity has been recognized. As a consequence, considerable effort has gone into characterizing protein/peptide side-chain and backbone motions, principally through temperature-dependent X-ray diffraction, NMR relaxation and amide exchange studies, and molecular dynamics simulations. NMR relaxation, in particular, is sensitive to a broad range of time scales. While measurement of most commonly used proton relaxation data can be acquired with rather good accuracy, the interpretation of such experimental data is complicated by the presence of multiple interproton motional vectors which are involved in deriving spectral densities.[1] An additional, nontrivial problem in interpreting these data lies in fully describing peptide bond rotations through the choice of an appropriate motional model. Numerous parameters are nec-

[‡]This work was made possible by a National Research Council/National Science Foundation International (U.S.S.R.) Project Development Grant to K.H.M. and benefitted from NMR facilities made available through Grant RR-04040 from the National Institutes of Health.
[†]Abbreviations: NMR, nuclear magnetic resonance; 2D-NMR, two-dimensional NMR spectroscopy; COSY, correlated spectroscopy; NOESY, nuclear Overhauser effect spectroscopy; NOE, nuclear Overhauser effect; rf, radio frequency; FID, free induction decay; IV-H1, parent peptide GVKGDKGNPGWPGAPY from type IV collagen; T_1, spin-lattice relaxation time; T_1(i), T_1 of ^{13}C-multiplet inner line (no proton decoupling); T_1(o), T_1 of ^{13}C-multiplet outer line (no proton decoupling); T_1, T_1 with proton decoupling.
[§]On leave from the Institute of Chemical Physics, Academy of Sciences of the USSR, 117977 Moscow, USSR.

(1) Torda, A. E.; Norton, R. S. *Biopolymers* **1989**, *28*, 703-716.

0002-7863/92/1514-4326$03.00/0

essary to describe the motions of the peptide chain and its multiple internal rotations. Therefore, only the simplest models have been used to interpret NMR relaxation data.[2-4]

NMR relaxation is usually dominated by internuclear dipole–dipole interactions which are proportional to the inverse sixth power of the internuclear distance and the rotational correlation time. If the internuclear distance term were independently known, the motional contribution could be more easily and accurately determined from relaxation data. This is generally the case for ^{13}C-NMR relaxation where dipole–dipole interactions with directly bonded proton(s) dominate the relaxation phenomenon. The interpretation of ^{13}C-NMR relaxation data for a methine group is thereby simplified. ^{13}C-Enriched samples allow good NMR sensitivity and have been used to accurately measure relaxation times and NOE coefficients.[5,6] However, the problem of choosing an appropriate motional model and fitting it with a limited number of experimental parameters still remains. ^{13}C-NMR relaxation studies are most frequently analyzed in terms of autocorrelation functions alone. A number of groups,[7-11] however, have shown that the analysis of cross-correlation spectral density terms in the relaxation of ^{13}C multiplet NMR spectra for CH_2 and CH_3 groups can give additional characteristics for molecular rotational motions. Fuson and Prestegard[4] have used this approach, for example, to analyze motions executed by a fatty acyl chain in phospholipid vesicles. Recently, an attempt to take into account cross-correlation terms for proton 2D-NMR spectra of a protein was made,[12] but as far as we know, there are no published papers on ^{13}C-multiplet relaxation in proteins/peptides.

For this initial study, we have chosen to investigate the rotational motions at glycine $^{13}CH_2$ (enriched) positions in collagen type IV peptide IV-H1, i.e., GVKGDKGNPGWPGAPY.[13] The five glycine CH_2 groups provide good probes of peptide backbone motions which can be modeled by analysis or by using ^{13}C multiplet relaxation and NOE data. Peptide IV-H1 was chosen for this and future studies for several reasons: (1) it has a relatively well-defined, average multiple turn conformation;[14] (2) it is a relatively short peptide that can be easily synthesized by solid-phase methods; (3) ^{13}C-enriched amino acids can be selectively incorporated at various positions along the chain; and (4) it has a glycine–XX repeat motif and contains three proline residues, these groups being more representative of peptide backbone motions.

Methods and Materials

Peptide Synthesis. Peptides representing amino acid sequences from human type IV collagen were synthesized on a Beckman 990 peptide synthesizer by Dr. Marek Kloczewiak, at the Shriners Burn Institute, Boston, MA. ^{13}C-Enriched glycine (Merck Sharpe & Dohme) was used in place of normal glycine. The peptide synthesis procedures used were based on the Merrifield solid-phase system as described elsewhere.[15] Lyophilized, crude peptides were purified by preparative reverse-phase HPLC on a C-18 column, using an elution gradient of 0–60% acetonitrile with 0.1% trifluoroacetic acid in water. The purity and composition of the peptides were verified by peptide sequencing and reverse-phase HPLC analysis.

NMR Spectroscopy. Freeze-dried samples for NMR measurements were dissolved in D_2O. Protein concentration was 7 mg/mL. pH was adjusted to pH 6 by adding microliter quantities of NaOD or DCl to the protein sample. The temperature was varied from 298 to 350 K. All NMR spectra were acquired on a General Electric QE-300 spectrometer at the ^{13}C frequency of 75 MHz.

T_1 measurements were performed by using the inversion–recovery pulse sequence. The acquisition number was chosen to give a signal to noise ratio greater than 5; therefore, the number of transients varied from 64 to 2048. Ten time incremented (partially relaxed) spectra were routinely acquired for each T_1 experiment. NOE measurements were made by using the gated decoupling pulse sequence with a time delay of more than $10T_1$ in order to minimize experimental error.[16]

Theory

Relation between Molecular Motion and ^{13}C-NMR Relaxation. Since NOE values as obtained herein have not reached their maximum limit, the extreme narrowing approximation could not be used for analysis of these ^{13}C relaxation data. Kuhlman, Grant, and Harris[17] have pointed out that the NOE coefficient decreases to 0.153 when rotational reorientation is slow, i.e., $\omega_C\tau_0 \gg 1$, where ω_C is the ^{13}C resonance frequency in radians/s and τ_0 is the rotational correlation time. Doddrell, Glushko, and Allerhand[2] have considered the more general case where $\omega_C\tau_0 \approx 1$ and have calculated NOE coefficients and spin–lattice (T_1) and spin–spin (T_2) relaxation times for spherical and symmetric top rotations. Their calculations, however, are only valid for the methine (–CH) group since cross-correlation effects, which are important for spin systems containing three or more nuclei,[7,8] were not considered. Werbelow and Grant[18] have derived such expressions for NOE coefficients, and the use of ^{13}C-multiplet relaxation of methylene and methyl groups has been reviewed by Werbelow and Grant.[8] A straightforward way to determine cross-correlation times is from the initial slope of relaxation curves for inner and outer ^{13}C multiplet lines.[19] In short, the influence of cross-correlation on ^{13}C relaxation is significant and must be taken into account when considering ^{13}C relaxation data.

How can one derive information about molecular motion from a consideration of cross-correlation effects in ^{13}C-NMR relaxation experiments? To answer this question, let us consider the main equations describing the NOE and T_1 relaxation for the CH_2 group.[8] For proton decoupled ^{13}C relaxation, one can write:

$$1/T_1 = KJ_{CH}^*(\omega_C) \tag{1}$$

with

$$K = 2\gamma_C^2\gamma_H^2\hbar^2/r_{CH}^6 \tag{2}$$

$\hbar$ is Planck's constant divided by 2π; r_{CH} is the internuclear distance between carbon and its bonded hydrogen; γ_C and γ_H are the magnetogyric ratios for carbon and hydrogen nuclei, respectively.

$$J_{CH}^*(\omega) = {}^3/_{10}[{}^1/_3 J_{CH}(\omega_H - \omega_C) + J_{CH}(\omega_C) + 2J_{CH}(\omega_C + \omega_H)] \tag{3}$$

where ω_H and ω_C are the ^1H and ^{13}C resonance frequencies, respectively, in radians/s and

$$J_{CH}(\omega) = 4\pi \int_0^\infty \langle Y_2^0(\Theta_{CH}(t))Y_2^0(\Theta_{CH}(0))\rangle \cos \omega t \, dt \tag{4}$$

This is the well-known spectral density function. Y_2^0 is the second-rank spherical harmonic; Θ_{CH} is the angle between the CH vector and, for example, the direction of the static magnetic field. At the extreme narrowing limit, i.e., frequency independent spectral densities, $J_{CH}(0) = \tau_{CH}$ which is the autocorrelation time

(2) Doddrell, D.; Glushko, V.; Allerhand, A. *J. Chem. Phys.* **1972**, *56*, 3683–3689.
(3) Gotlib, Y. Y.; Neelov, I. M.; Torchinsky, I. A.; Shevelev, V. A. *Acta Polymer* **1989**, *40*, 643–648.
(4) Fuson, M. M.; Prestegard, J. H. *J. Am. Chem. Soc.* **1983**, *105*, 168–176.
(5) McCain, D. C.; Ulrich, E. L.; Markley, J. L. *J. Magn. Reson.* **1988**, *80*, 296–305.
(6) Sherry, A. D.; Keepers, J.; James, T. L.; Teherani, J. *Biochemistry* **1984**, *23*, 3181–3185.
(7) Daragan, V. A.; Khazanovich, T. N.; Stepanyants, A. U. *Chem. Phys. Lett.* **1974**, *26*, 89–92.
(8) Werbelow, L. G.; Grant, D. M. *Adv. Magn. Reson.* **1977**, *9*, 189–301.
(9) Vold, R. L.; Vold, R. R. *Prog. NMR Spectrosc.* **1978**, *12*, 79–95.
(10) Mayne, C. L.; Grant, D. M.; Alderman, D. W. *J. Chem. Phys.* **1976**, *65*, 1684–1692.
(11) Fuson, M. M.; Prestegard, J. H. *J. Chem. Phys.* **1982**, *76*, 1539–1549.
(12) Brueschweiler, R.; Griesinger, C.; Ernst, R. R. *J. Am. Chem. Soc.* **1989**, *111*, 8034–8035.
(13) Chelberg, M. K.; McCarthy, J. B.; Skubitz, A. P. N.; Furcht, L. T.; Tsilibary, E. C. *J. Cell Biol.* **1990**, *111*, 261–270.
(14) Mayo, K. H.; Parra-Diaz, D.; Chelberg, M.; McCarthy, J. *Biochemistry* **1991**, *30*, 8251–8267.
(15) Stewart, J. M.; Young, J. D. *Sold Phase Peptide Synthesis*, 2nd ed.; Pierce Chemical Co.: Rockford, IL, 1984; pp 135.
(16) Canet, D. *J. Magn. Reson.* **1976**, *23*, 361–364.
(17) Kuhlman, K. F.; Grant, D. M.; Harris, R. K. *J. Chem. Phys.* **1970**, *52*, 3439–3443.
(18) Werbelow, L. G.; Grant, D. M. *J. Chem. Phys.* **1975**, *63*, 4742–4749.
(19) Daragan, V. A.; Khazanovich, T. N. In *Magnetic Resonance and Related Phenomena*; Springer-Verlag: Heidelberg, 1979; p 475.

for the reorientation of the CH vector with respect to the laboratory frame. Here we shall assume that the intramolecular dipole–dipole interaction dominates the overall relaxation process.

The NOE coefficient is defined as $n = (I - I_0)/I_0$. I and I_0 are the line intensities for proton irradiated and nonirradiated cases, respectively;

$$n = \tfrac{1}{2}(\gamma_H/\gamma_C)[(A_1A_2 - A_3A_4)/(A_1A_5 - A_3^2)] \quad (5)$$

where

$$A_1 = \tfrac{1}{3}[\tfrac{8}{3}(J_{CH}(0) - J_{HCH}(0)) + A_5 + 4(J_{CH}(\omega_H) - J_{HCH}(\omega_H))]$$

$$A_2 = 4[2J_{CH}(\omega_C + \omega_H) - \tfrac{1}{3}J_{CH}(\omega_C - \omega_H)]$$

$$A_3 = \tfrac{2}{3}^{1/2}(\tfrac{1}{3}J_{HCH}(\omega_C - \omega_H) + J_{HCH}(\omega_C) + 2J_{HCH}(\omega_C + \omega_H))$$

$$A_4 = \tfrac{4}{3}^{1/2}(2J_{HCH}(\omega_C + \omega_H) - \tfrac{1}{3}J_{HCH}(\omega_C - \omega_H))$$

$$A_5 = \tfrac{20}{3}J_{CH}^*(\omega)$$

The importance of the cross-correlation terms, $J_{HCH}(\omega)$, on the NOE coefficient is apparent:

$$J_{HCH}(\omega) = 4\pi\int_0^\infty \langle Y_2^0(\Theta_{CH}(t))Y_2^0(\Theta_{CH'}(0))\rangle \cos \omega t\, dt \quad (6)$$

where CH and CH′ are the two CH vectors of the CH_2 group.

From NOE data alone, however, it is difficult to determine the cross-correlation spectral density, J_{HCH}, even at the extreme narrowing limit, and it is necessary to consider ^{13}C multiplet relaxation. Based on equations given by Werbelow and Grant,[18] it is possible for inversion–recovery experiments to show that the initial relaxation rates of inner, i.e., $1/T_1(i)$, and outer, i.e., $1/T_1(o)$, lines of the ^{13}C triplet (^1H-coupled) spectrum can be described by:

$$1/T_1(i) = K(J_{CH}^*(\omega) - \tfrac{3}{10}J_{HCH}(\omega_C)) \quad (7)$$

and

$$1/T_1(o) = K(J_{CH}^*(\omega) + \tfrac{3}{10}J_{HCH}(\omega_C)) \quad (8)$$

i.e.,the cross-correlation spectral density can be easily determined from:

$$J_{HCH}(\omega_C) = \tfrac{5}{6}[r_{CH}^6/\gamma_C^2\gamma_H^2\hbar^2](1/T_1(o) - 1/T_1(i)) \quad (9)$$

By using this equation, even a linear approximation at the half-intensity change in the inversion–recovery relaxation experiment gives an error of less than 5% in determining $J_{HCH}(\omega_C)$.[19] It should be noted that this method of determining cross-correlated spectral densities is more straightforward than using the normally employed method of fitting a set of relaxation curves.

Now let us consider the relation between ^{13}C relaxation parameters and molecular motion. In the simplest case of the spherical top rotation with no internal motion, one can show that:

$$J_{CH}(\omega) = \tau_o/(1 + \omega^2\tau_o^2) \quad (10)$$

and

$$J_{HCH}(\omega) = \tfrac{1}{2}(3\cos^2\alpha - 1)(\tau_o/(1 + \omega^2\tau_o^2)) \quad (11)$$

where α is the angle between the two CH bonds, and the overall rotational correlation time, $\tau_o = 1/(6D)$, where D is the rotational diffusion coefficient. For a tetrahedral CH_2 group configuration,

$$J_{HCH}(\omega) = -\tfrac{1}{3}J_{CH}(\omega) \quad (12)$$

If we assume that $r_{CH} = 1.09$ Å, we can calculate the auto- and cross-correlation spectral densities, NOE coefficients, and T_1 values for inner (i) and outer (o) lines of the ^{13}C multiplet, i.e., $T_1(i)$ and $T_1(o)$, respectively, and T_1 for the proton decoupled case for different values of τ_o. The data are presented in the Results section. For this calculation, we have used the value $\omega_C/2\pi = 75$ MHz.

It is apparent that differences among $T_1(i)$, $T_1(o)$, and T_1 values may be significant, and therefore one can determine cross-correlation spectral densities from these ^{13}C relaxation experiments. It is important to note that in the case of isotropic rotation, $T_1(o) > T_1(i)$ for all calculated τ_o values. (Note that $T_1^{-1} = \tfrac{1}{2}(T_1(o)^{-1} + T_1(i)^{-1})$.) If the rotational reorientation is anisotropic, the relations between NOE, $T_1(o)$, and $T_1(i)$ will be considerably more complex. For simplicity, we shall only consider rotation of a symmetric top. The internal rotation of a CH_2 group attached to a body undergoing isotropic reorientation can be described by the same equations. Woessner[20] and Werbelow and Grant[8] have shown that in the case of diffusional reorientation, the spectral densities are given by:

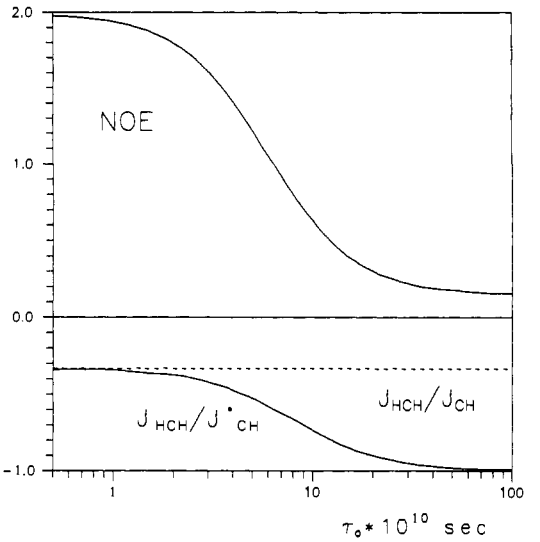

Figure 1. NOE coefficient and spectral density ratios. The calculated NOE coefficient and the ratios $J_{HCH}(\omega_C)/J_{CH}^*(\omega)$ and $J_{HCH}(\omega)/J_{CH}(\omega)$ for the isotropic reorientation of the methylene tetrahedral group. The Larmor precession frequency for ^{13}C nuclei is 75 MHz.

$$J_{CH}(\omega) = At_1(\omega) + Bt_2(\omega) + Ct_3(\omega) \quad (13)$$

and

$$J_{HCH}(\omega) = A't_1(\omega) + B't_2(\omega) + C't_3(\omega) \quad (14)$$

where

$$A = \tfrac{1}{4}(3\cos^2\Theta_{CH} - 1)^2$$

$$B = 3\cos^2\Theta_{CH}\sin^2\Theta_{CH}$$

$$C = \tfrac{3}{4}\sin^4\Theta_{CH}$$

$$A' = \tfrac{1}{4}(3\cos^2\Theta_{CH} - 1)(3\cos^2\Theta_{CH'} - 1)$$

$$B' = 3\cos\Theta_{CH}\cos\Theta_{CH'}\sin\Theta_{CH}\sin\Theta_{CH'}\cos(\phi_{CH'} - \phi_{CH})$$

$$C' = \tfrac{3}{4}\sin^2\Theta_{CH}\sin^2\Theta_{CH'}\cos(2\phi_{CH'} - 2\phi_{CH})$$

$$t_1(\omega) = 6D_\perp/[(6D_\perp)^2 + \omega^2]$$

$$t_2(\omega) = (5D_\perp + D_\parallel)/[(5D_\perp + D_\parallel)^2 + \omega^2]$$

$$t_3(\omega) = (2D_\perp + 4D_\parallel)/[(2D_\perp + 4D_\parallel)^2 + \omega^2]$$

Here, $D_\perp$ and $D_\parallel$ are the components of the diagonalized rotational diffusion tensors ($D_{zz} = D_\parallel$, and $D_{xx} = D_{yy} = D_\perp$). Θ_{CH}, ϕ_{CH}, $\Theta_{CH'}$, and $\phi_{CH'}$ are the conventional polar and azimuthal angles that position the CH and CH′ vectors with respect to the principal axis of the molecular diffusional rotating frame.

Results and Discussion

From the theory presented above, Figure 1 gives the calculated NOE and the ratio $J_{HCH}(\omega_C)/J_{CH}^*(\omega)$ dependencies on $\tau_o = 1/(6D)$, the correlation time of the isotropic rotational motion. This ratio can be easily determined from these experiments by using eqs 1, 7, and 8. As previously mentioned, calculations were

(20) Woessner, D. E. *J. Chem. Phys.* **1962**, *36*, 1–8.

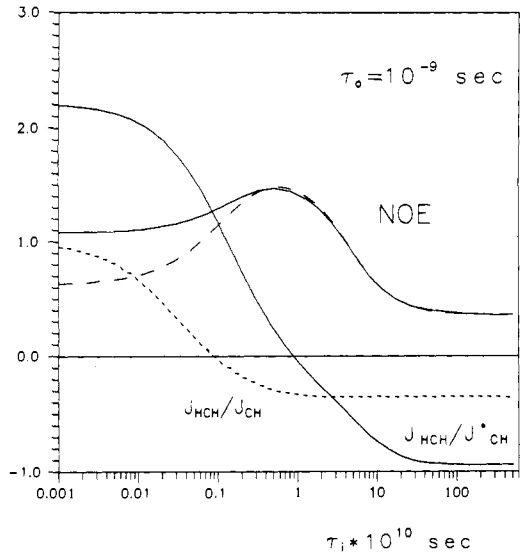

Figure 2. NOEs and spectral density ratios for symmetric top rotation. Calculated NOE coefficients and the ratios $J_{HCH}(\omega_C)/J_{CH}^*(\omega)$ and $J_{HCH}(\omega)/J_{CH}(\omega)$ for the symmetric top rotation of the methylene tetrahedral group. Larmor precession frequency for ^{13}C nuclei is 75 MHz. Angles between CH vectors and the molecular z-axis of the rotational frame are tetrahedral. The dashed line indicates the NOE coefficient without cross-correlation terms (methine group). The correlation time for z-axis reorientation $\tau_o = {}^1/_6D_\perp = 10^{-9}$ s; $\tau_i = {}^1/_6D_\parallel$.

made for $\omega_C/2\pi = 75$ MHz. Note that, at the extreme narrowing limit for CH_2 group tetrahedral geometry, the ratio $T_1(i)/T_1(o) = 0.82$ (see eqs 7, 8, and 9). For $\tau_o > 2 \times 10^{-9}$ s, $T_1(i)/T_1(o) = 0.54$. This means that the multiplet effect (the difference in initial relaxation rates of the outer and inner lines of ^{13}C-NMR multiplet from the inversion recovery experiment) is more pronounced for slower motions. For comparison, Figure 1 also gives the ratio of cross- to autocorrelation spectral densities, $J_{HCH}(\omega)/J_{CH}(\omega)$, which most frequently appears in the literature. We have chosen to plot $J_{HCH}(\omega)/J_{CH}^*(\omega)$ because this ratio follows more clearly from experiment where $(1/T_1)_{dipolar}$ is represented by $J_{CH}^*(\omega)$.

Figure 2 gives the calculated NOE and the ratio $J_{HCH}(\omega_C)/J_{CH}^*(\omega)$ for the case where internal rotation of the tetrahedral CH_2 group has been included. This case is described by eqs 13 and 14, where $6D_\perp = 1/\tau_o$ and $6D_\parallel = 1/\tau_i$. τ_i is the correlation time for internal rotation. $J_{HCH}(\omega)/J_{CH}(\omega)$ is again shown for comparison. Calculations were done for a τ_o value of 10^{-9} s since, as shall be shown later in this paper, the experimentally derived τ_o value is in this range. The strong dependence of the multiplet effect on τ_i is apparent. For small values of τ_i ($<10^{-12}$ s), the ratio of initial relaxation rates $T_1(i)/T_1(o) = 4.9$. At the other extreme, if the internal motion is restricted ($\tau_i > 2 \times 10^{-9}$ s), $T_1(i)/T_1(o) \approx 0.54$. In contrast to this case, it is important to realize that, for the extreme narrowing condition, $J_{CHH}(0)/J_{CH}^*(0)$ which is equal to $J_{HCH}(0)/J_{CH}(0)$, is limited to values from 1 to −0.33 for both small and large ratios of τ_i/τ_o (see, for example, Hartzell et al.[21]) and $T_1(i)/T_1(o)$ variations are not as large. Even at this point, it is obvious that the ^{13}C multiplet effect is a sensitive method for studying peptide/protein internal motions.

Figure 2 also shows the influence of cross-correlation terms on the value of the NOE coefficient. One can see that the difference between the NOE coefficient with (solid line) and without (dashed line) cross-correlation may be more than 30% when τ_i is very small. The methine (CH−) group is an example where cross-correlation would not have to be taken into account.

It is also interesting to consider the influence of the orientation of the CH_2 group (with respect to the molecular rotational frame) on the NOE and ^{13}C multiplet relaxation data. Figure 3 shows the theoretical dependence of the NOE, $J_{CH}^*(\omega)$, and cross-

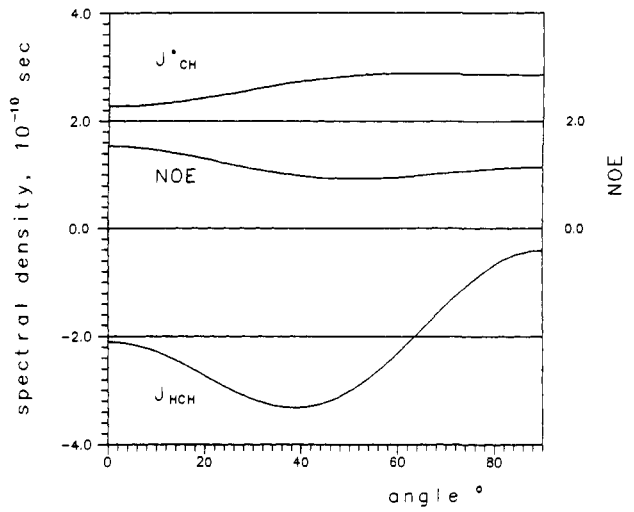

Figure 3. NOEs and spectral density ratios for symmetric top rotation. Calculated NOE coefficients and the ratio $J_{HCH}(\omega_C)/J_{CH}^*(\omega)$ for the symmetric top rotation of the methylene tetrahedral group. Larmor precession frequency for ^{13}C nuclei is 75 MHz. $\tau_o = {}^1/_6D_\perp = 10^{-8}$ s. $\tau_i = {}^1/_6D_\parallel = 10^{-10}$ s. The z-axis of the rotational frame lies in the HCH plane. "Angle" is the angle between the z-axis and the HCH angle bisector.

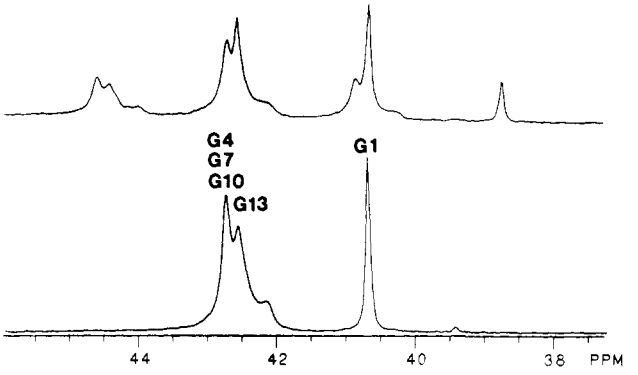

Figure 4. ^{13}C-NMR spectra of collagen type IV peptide IV-H1. Two ^{13}C-NMR (75 MHz) spectra of peptide IV-H1 are shown with broad band proton decoupling (below) and nondecoupled (above). The peptide concentration is 7 mg/mL. The solution pH was adjusted to pH 6, and the temperature was 35 °C. Other conditions are as discussed in the text.

correlational ($J_{HCH}(\omega_C)$) spectral densities on the angle between the z-axis of the molecular rotational frame and the HCH angle bisector. Note that if $\Theta_{CH} \neq \Theta_{CH'}$, one should use the average values A, B, and C in eqs 13 and 14; $A \rightarrow {}^1/_2(A(\Theta_{CH}) + A(\Theta_{CH'}))$, and so on. Here, it is assumed that $\tau_o = 1/(6D_\perp) = 10^{-9}$ and $\tau_i = 1/(6D_\parallel) = 10^{-10}$ s. The z-axis of the rotational frame lies in the HCH plane. In Figure 3, one can see that the cross-correlation spectral density is much more sensitive to this angle than are the autocorrelation $J_{CH}^*(\omega)$ and NOE terms.

Now we shall consider some experimental results. The proton decoupled ^{13}C-NMR spectrum (75 MHz) for the ^{13}C-glycine enriched peptide IV-H1 is shown in the lower spectral trace of Figure 4. Since ^1H-NMR sequence-specific assignments have been made for the peptide,[14] a heteronuclear ^{13}C–^1H two-dimensional correlated spectroscopy (COSY) experiment (data not shown) allowed assignment groupings of ^{13}C-glycine resonances. Some ambiguities remained, however, due to overlap of G1, G7, and G10 αH resonances and cis–trans proline isomer-induced conformational populations for G7, G10, and G13. Based on the heteronuclear two-dimensional COSY spectrum, however, the most upfield, apparently single ^{13}C-glycine resonance at 41.2 ppm can only be assigned to either G1, G7, or G10. However, since it resonates more upfield and demonstrates a significantly narrower line width than the other glycine resonances, it may be assigned to the N-terminal glycine, G1. A backbone ^{13}C positioned at the

(21) Hartzell, C. J.; Stein, P. C.; Lynch, T. J.; Werbelow, L. G.; Earl, W. L. *J. Am. Chem. Soc.* **1989**, *111*, 5114–5119.

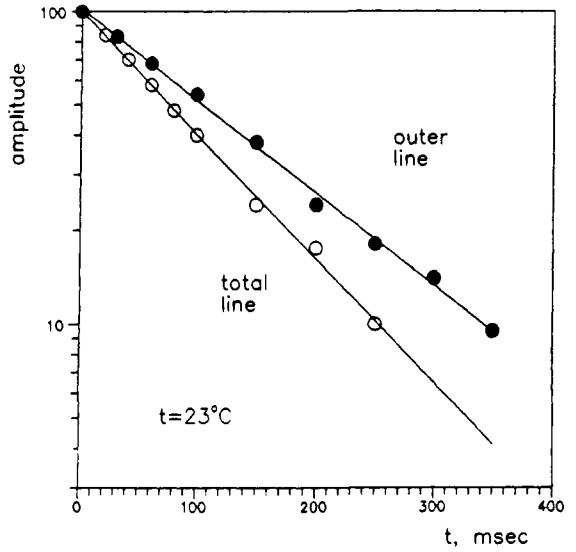

Figure 5. ^{13}C-NMR relaxation curves. Relaxation curves of the first line of the ^{13}C-NMR spectrum of the CH_2 group. Open circles are for relaxation measurements done with broad band proton decoupling; closed circles have been done without decoupling. The temperature was 23 °C; the pH was 6 and the peptide concentration was 7 mg/mL.

N-terminus of a peptide usually resonates more upfield than those found at nonterminal positions. Since G13 proton resonances are upfield ring current shifted,[2] correlation with ^{13}C resonance frequencies in the heteronuclear NMR experiment identifies the G13 ^{13}C resonance as labeled in Figure 4. The remaining resonances must, therefore, be assigned to the remaining three nonterminal glycines, i.e., G4, G7, and G10. These assignments have been indicated in Figure 4. Some minor ^{13}C-glycine resonances (not labeled in the figure) are due to the presence of cis proline isomers as noted by Mayo et al.[14]

In the upper part of Figure 4, the same ^{13}C spectral region is shown for the proton coupled spectrum. The multiplet pattern is easily recognized because ^{13}C–^{1}H coupling constants for the methylene group are about 150 Hz. Since overlap of some outer and inner multiplet lines is apparent, relaxation rate measurements of the inner lines for the $^{13}CH_2$ triplet were not possible. Outer resonances, however, are sufficiently resolved to allow multiplet relaxation to be studied. Therefore, relaxation experiments were limited to outer lines for proton coupled spectra and to lines for decoupled spectra. From eqs 3 and 9, it is apparent that this information is enough to calculate auto- and cross-correlation spectral densities, $J_{CH}^*(\omega)$ and $J_{HCH}(\omega_C)$, respectively. Moreover, NOE coefficients, which give additional insight into motional characteristics, will be discussed later.

For temperatures less than 40 °C, the relaxation rates of the three most downfield ^{13}C resonance envelopes (decoupled) are approximately equal, and in this paper we shall not separate the relaxation behavior of this part of the ^{13}C spectrum. Therefore, we shall consider only relaxation of the most downfield resonance in this group as representative of all nonterminal glycines (also called "body" glycines), and the most upfield ^{13}C resonance which has been assigned to the terminal glycine, G1.

Examples of the ^{13}C NMR inversion recovery relaxation curves for proton coupled (outer lines of the ^{13}C multiplet) and decoupled (total line) spectra are shown in Figure 5 for data acquired at 23 °C. These curves represent data for the nonterminal glycines. Both curves were fit with a single exponential; therefore, there was no problem to determine the initial slopes, $1/T_1(o)$ and $1/T_1$, from these experiments. It is obvious from this figure that T_1 is less than $T_1(o)$. From eqs 3 and 9, it is clear that the cross-correlation spectral densitity for this nonterminal glycine resonance is negative. For the terminal glycine, on the other hand, T_1 is greater than $T_1(o)$, indicating a positive sign for the cross-correlation term. The results of measuring $T_1(o)$ and T_1 for terminal and nonterminal (body) glycines are presented in Figure 6 for the temperature range 23 °C to 75 °C. Simple linear least-squares

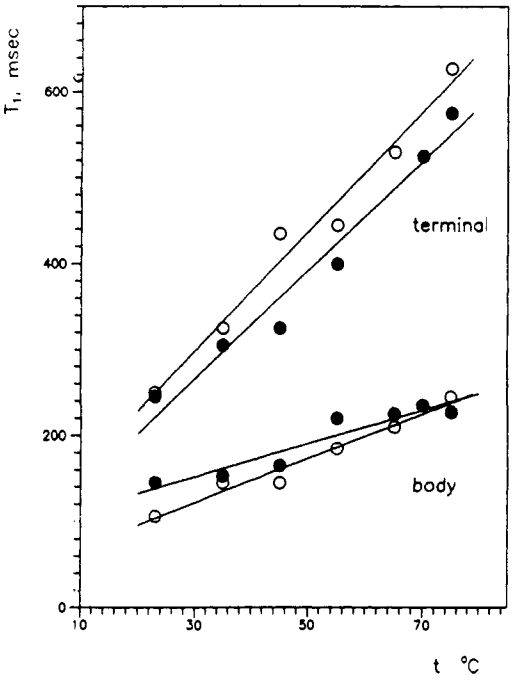

Figure 6. Temperature dependence of T_1. Temperature dependence of T_1 for the first (body) glycine line and for the fourth (terminal) glycine line of the ^{13}C-NMR spectrum of peptide IV-H1 are shown. Black circles are for the outer line of the ^{13}C-triplet spectrum of the CH_2 group, ($T_1(o)$) and open circles are for the broad band proton decoupled line. Conditions are the same as described in the Figure 5 legend.

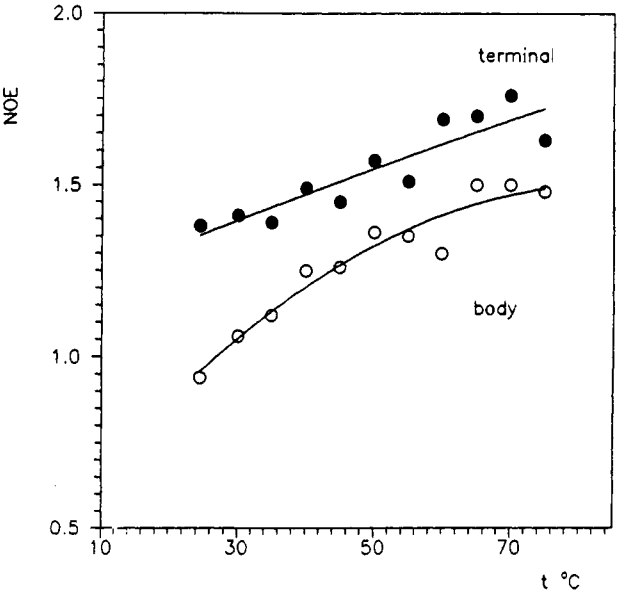

Figure 7. NOE temperature dependence. Temperature dependence of the NOE coefficients for the first (body) and the fourth (terminal) glycine lines of the ^{13}C-NMR spectrum of peptide IV-H1. Conditions are the same as described in the Figure 5 legend.

fits are used. The results of these fits for nonterminal glycines are:

$$T_1(o) = 1.944t + 93.51$$

$$T_1 = 2.581t + 44.48$$

and for the terminal glycine:

$$T_1(o) = 6.349t + 75.21$$

$$T_1 = 6.972t + 89.08$$

where t is in degrees Celsius, and T_1 and $T_1(o)$ values are in milliseconds.

Table I. Temperature Dependence of the Auto- and Cross-correlation-Spectral Densities

		temp, °C			
		25	35	55	75
body	$J_{CH}^*(\omega)$	2.16[a]	1.74	1.27	0.99
glycine	$J_{HCH}(\omega_C)$	−1.67	−0.97	−0.29	−0.01
	$J_{HCH}(\omega_C)/J_{CH}^*(\omega)$	−0.77	−0.56	−0.23	−0.01
terminal	$J_{CH}^*(\omega)$	0.89	0.71	0.50	0.38
glycine	$J_{HCH}(\omega_C)$	0.37	0.28	0.19	0.14
	$J_{HCH}(\omega_C)/J_{CH}^*(\omega)$	0.41	0.40	0.38	0.37

[a] All spectral densities are in increments of 10^{-10} s.

Measured NOE coefficients shown in Figure 7 increase with increasing temperature. These data indicate that, even at relatively high temperatures, the extreme narrowing condition is not met. Solid curves in this figure are the result of parabolic approximations.

The opposite signs of cross-correlation spectral densities and significantly different NOE coefficients for terminal and nonterminal glycine signals indicate the varied character of methylene group motions at these glycine positions along the peptide chain. One can see from Figures 1–3 that a positive sign for $J_{HCH}(\omega_C)$ indicates significant anisotropic rotation of the CH_2 group of the terminal glycine relative to nonterminal glycine positions. The results of calculating auto- and cross-correlation spectral densities are presented in Table I. Here one can see that, for the terminal glycine, the ratio of the cross- and auto-correlation spectral densities is independent of temperature within experimental error. This means that the activation energy for internal rotation and for reorientation of the z-axis of internal rotation are approximately equal.

A Model for Terminal Glycine Motions. For a better molecular motional description of the terminal glycine G1, we have considered a simple model involving internal rotation of G1 around the C_α—C=O bond with correlation time τ_i and isotropic reorientation of this bond having correlation time τ_o. For this analysis, it has been assumed that the angles between CH vectors of the CH_2 group and the C_α—C=O bonds are tetrahedral and that the C–H bond distance is 1.09 Å. We have fitted T_1, $T_1(o)$, and NOE data and obtained (at 23 °C): $\tau_o = (9.2 \pm 0.5) \times 10^{-10}$ s and $\tau_i = (0.16 \pm 0.3) \times 10^{-10}$ s. The general temperature dependencies of τ_o and τ_i indicate typical Arrhenius behavior with activation energies $E_o = (20 \pm 3)$ kJ/mol and $E_i = (18 \pm 4)$ kJ/mol for τ_o and τ_i, respectively. These data are in agreement with the result from cross-correlation spectral densities mentioned earlier, i.e., no temperature dependence of the ratio $J_{HCH}(\omega_C)/J_{CH}^*(\omega)$.

From these data it is apparent that G1 rotates highly anisotropically. This may have been expected since G1 is at a terminal position where, as a qualitative first approximation, relatively fast rotation around the C_α—C=O bond usually occurs in addition to isotropic reorientation of the C_α—C=O bond. Interestingly, the time scale of the G1 internal rotation is 10–20 ps, which falls in the same range normally sampled by molecular dynamics simulations.

A Model for Nonterminal Glycine Motions. Since all other, nonterminal glycines demonstrate approximately equal relaxation characteristics, and since their T_1 values are less than their $T_1(o)$ values, i.e., negative sign of the cross-correlation spectral density, they can be expected to move more isotropically than G1 and with a more relatively fixed orientation of the CH_2 group with respect to the molecular rotational frame. In effect, this indicates significantly less internal motion at these chain positions. This observation is consistent with two-dimensional proton NMR NOESY data[14] that give a better defined set of relatively larger short- and long-range NOEs for sequences around G7, G10, and G13. A quantitative interpretation of the experimental data for nonterminal glycines, however, is more complicated. Obviously a more realistic model for molecular motion is necessary to take into account this added complexity. Such a model must consider multiple internal rotations and asymmetric overall rotation of the molecule as a whole. For the present, these data will be interpreted simply in the context of symmetric top molecular rotation.

From Figure 1, it can be shown that spherical top rotation cannot simultaneously describe the nonterminal glycine experimental values for NOE coefficients and the ratio $J_{HCH}(\omega_C)/J_{CH}^*(\omega)$. Moreover, the model which we have used above to interpret data for the terminal glycine case is not applicable at all temperatures for nonterminal glycines. Considering the symmetric top rotation model, the only way to fit the experimental data for nonterminal glycines is to consider the orientation of the CH_2 group with respect to the molecular rotational frame as one of the fitting parameters.

Since a simple relationship exists between the spherical polar angles θ_1, ϕ_1 and θ_2, ϕ_2 for C–H_i bond vectors ($i = 1, 2$),

$$\cos(\phi_2 - \phi_1) = [\cos(\mathrm{HCH}) - \cos\theta_1 \cos\theta_2]/[\sin\theta_1 \sin\theta_2] \quad (15)$$

only two angles, θ_1 and θ_2, are needed to describe the rotational characteristics for the CH_2 group in this case. Since we only have three experimental parameters, i.e., $T_1(o)$, T_1, and NOE, for the determination of four model parameters, i.e., τ_o, τ_i, Θ_1, and Θ_2, we can only consider some useful limitations for Θ_1 and Θ_2 angles.

Computational analysis shows that in order to fit the experimental data over all temperatures, i.e., 23–75 °C, θ_1 and θ_2 must be near 60° and 150°, respectively, and τ_i must be at least two times greater than for the terminal glycine G1. The large variation of the ratio $J_{HCH}(\omega_C)/J_{CH}^*(\omega)$ with temperature indicates, moreover, that the character of internal rotation for nonterminal glycines varies with temperature more drastically than it does for the terminal glycine. As the temperature is increased, anisotropy of the rotational motions in the peptide backbone increases; this in turn indicates relative "melting" of the preferred, multiple turn structure in the peptide.[14] Preferred structure, however, does not mean invariable, and since this short linear peptide most probably exists in a number of fluctuating conformation states, the "melting" curve is not sharp. Therefore, apparent "melting" is reflected in a convergence of inner and outer line relaxation temperature dependencies.

Based on this model, the ratio $D_\parallel/D_\perp$ which best fits the data ranges from approximately 80 to 120. In this context, the molecule can be pictured as an ellipsoid that preferentially rotates about the long axis, i.e., z-axis as defined above. Surprisingly, our crude picture has much in common with the ^{1}H-NMR/NOE constrained modeled structure of peptide IV-H1[14] whose general molecular shape is that of an ellipsoid with z:y,y axial ratio of about 4:1. In other words, axial rotation about the z-axis would have to be approximately 20–30 times greater than that about the x,y-axes in order to explain the ratio $D_\parallel/D_\perp$. In the structural model, nonterminal glycines are, on average, oriented nearly normal to the long axis. Even though it is clear that motional models used in this study are able to explain general features and trends in these data, more complex rotational models, which incorporate internal rotations and correlation of these rotations, are needed.

In conclusion, we can say that ^{13}C-NMR/NOE and multiplet relaxation data are very sensitive to the details of molecular reorientation, internal motions, and molecular geometry. This approach provides a very useful method for investigating protein peptide structural dynamics.